© 2022. Published by The Company of Biologists Ltd | Development (2022) 149, dev199498. doi:10.1242/dev.199498

STEM CELLS AND REGENERATION

RESEARCH ARTICLE

Vascular endothelial growth factor c regulates hematopoietic stem cell fate in the dorsal aorta

Rebecca K. Schiavo* and Owen J. Tamplin*,‡

ABSTRACT

Hematopoietic stem and progenitor cells (HSPCs) are multipotent cells that self-renew or differentiate to establish the entire blood hierarchy. HSPCs arise from the hemogenic endothelium of the dorsal aorta (DA) during development in a process called endothelial-to-hematopoietic transition. The factors and signals that control HSPC fate decisions from the hemogenic endothelium are not fully understood. We found that Vegfc has a role in HSPC emergence from the zebrafish DA. Using time-lapse live imaging, we show that some HSPCs in the DA of *vegfc* loss-of-function embryos display altered cellular behavior. Instead of typical budding from the DA, emergent HSPCs exhibit crawling behavior similar to myeloid cells. This was confirmed by increased myeloid cell marker expression in the ventral wall of the DA and the caudal hematopoietic tissue. This increase in myeloid cells corresponded with a decrease in HSPCs that persisted into larval stages. Together, our data suggest that Vegfc regulates HSPC emergence in the hemogenic endothelium, in part by suppressing a myeloid cell fate. Our study provides a potential signal for modulation of HSPC fate in stem cell differentiation protocols.

KEY WORDS: VEGFC, Hematopoietic stem cells, Hemogenic endothelium, Hematopoiesis, Dorsal aorta, Zebrafish

INTRODUCTION

In vertebrates, hematopoiesis occurs in two waves, the primitive and definitive wave. The primitive wave occurs first, producing erythrocytes and macrophages to oxygenate and provide immune defense for the developing embryo. The definitive wave follows to produce long-term multipotent hematopoietic stem and progenitor cells (HSPCs) that can self-renew or differentiate to create all mature blood cells. Definitive HSPCs emerge from the hemogenic endothelium (HE) in the aorta-gonad-mesonephros (AGM) region through endothelial-to-hematopoietic transition (EHT) (Müller et al., 1994; Bertrand et al., 2010; Kissa and Herbomel, 2010; Boisset et al., 2010). HSPCs then migrate to seed their intermediary niche, the fetal liver (FL), which allows for expansion of the blood stem cell pool before settling in their adult niche, the bone marrow (Ema and Nakauchi, 2000). Hematopoietic development is difficult to observe in mammals because it occurs *in utero*.

Zebrafish are an excellent alternative model organism for the study of hematopoiesis. Their external and transparent development allows for *in vivo* visualization. In zebrafish, HSPCs emerge from the HE of the dorsal aorta (DA) and migrate to their intermediary niche, the caudal hematopoietic tissue (CHT) (Murayama et al., 2006; Tamplin et al., 2015), where they expand before colonizing the adult niche in the kidney marrow (Ciau-Uitz et al., 2014). Although much of the ontogeny of the hematopoietic system is conserved between mammals and zebrafish, differences exist. During mammalian emergence, HSPCs form intra-aortic hematopoietic clusters in the lumen of the DA before budding off into circulation and seeding the FL (Garcia-Porrero et al., 1995; Yokomizo and Dzierzak, 2010; Boisset et al., 2010). In zebrafish, HSPCs emerge from the ventral wall of the DA and migrate through the sub-aortic space to bud into the cardinal vein (Bertrand et al., 2010; Kissa and Herbomel, 2010).

Studies in mouse have shed light on the complex fate decisions arterial endothelial cells (ECs) must progress through to become an HSPC. The initial step is specification, when a subset of ECs in the DA begin to express hematopoietic markers Gfi1, Runx1 and Gata2, and become HE (North et al., 1999; Kobayashi-Osaki et al., 2005; Kang et al., 2018). Once the HE is specified, cells acquire expression of CD41 (also known as Itga2b) and c-KIT (Kit), then emerge into the lumen of the DA to form intra-aortic hematopoietic clusters (Boisset et al., 2010). Within the clusters, cells proximal to the wall of the DA display pre-hematopoietic stem cell (HSC) type I markers [CD45− (also known as Ptprc−), c-KIT^{low}] and are slowly cycling, whereas distal cells display pre-HSC type II markers (CD45+, c-KIT^{high}) and are more proliferative (Batsivari et al., 2017; Yokomizo and Dzierzak, 2010). Distally located cells mature to become definitive HSCs, and cell cycling slows before release into circulation and migration to the FL. Although the process of HSPC maturation and emergence has been described, there is a lack of knowledge of factors that may influence HSPC differentiation during EHT.

Human vascular endothelial growth factor c (VEGFC) is a major driver of lymphangiogenesis through its binding to VEGF receptor-2 (VEGFR2; KDR) and VEGFR3 (FLT4) (Stacker et al., 2014; Joukov et al., 1996). The essential function of Vegfc and its receptor Vegfr3 (Flt4) in lymphatic development is highly conserved in zebrafish (Shin et al., 2016; Le Guen et al., 2014; Villefranc et al., 2013). Proteolytic cleavage of human VEGFC is necessary for binding to VEGFR2 and VEGFR3 (Joukov et al., 1997). The secreted proteins involved in this post-translational processing, CCBE1 and ADAMTS3, are also conserved in zebrafish, with mutants showing similar lymphatic defects (Le Guen et al., 2014; Hogan et al., 2009; Wang et al., 2020). Interestingly, recent studies have shown evolutionary differences in the binding specificity of Vegfc in zebrafish (Vogrin et al., 2019). The single VEGFR2 receptor in placental mammals has two related proteins in zebrafish, Kdrl and Kdr, that both bind Vegfa and are required for vascular development (Covassin et al., 2006; Bahary et al., 2007). In zebrafish, Vegfc binds Vegfr3 and Kdr, but not Kdrl (Vogrin et al., 2019).

Department of Pharmacology, University of Illinois at Chicago, Chicago, IL 60612, USA.
*Present address: Department of Cell and Regenerative Biology, University of Wisconsin – Madison, Madison, WI 53705, USA.

‡Author for correspondence (tamplin@wisc.edu)

O.J.T., 0000-0001-9146-4860

Handling Editor: Hanna Mikkola
Received 4 February 2021; Accepted 6 December 2021

Development (2022) 149, dev199498. doi:10.1242/dev.199498

The role of VEGFC in hematopoiesis is still emerging and a few studies in mice have uncovered hematopoietic phenotypes. Recent studies have shown a role for Vegfc and Ccbe1 in FL erythropoiesis (Fang et al., 2016; Zou et al., 2013). Ccbe1-deficient mice are anemic, with impaired erythroblast proliferation and survival (Zou et al., 2013). Vegfc conditional knockout mice have decreased FL erythropoiesis and overall anemia (Fang et al., 2016). After irradiation, mice lacking Vegfc showed impaired hematopoietic regeneration and delayed vascular recovery of the bone marrow niche (Fang et al., 2020). A study of embryonic day (E) 9.5 para-aortic splanchnopleural mesoderm (P-Sp) explants from *Vegfr3*-deficient mouse embryos revealed reduced hematopoietic progenitor numbers (Hamada et al., 2000). Further analysis using this P-Sp explant model demonstrated competition between Vegfa and Vegfc for binding to both Vegfr3 and Vegfr2, resulting in synergistic regulation of hematopoietic and vascular development (Hamada et al., 2000). However, the role of VEGFC in specification of early definitive hematopoietic progenitors remains unclear.

Here, we reveal a previously unknown role for VEGFC in maintaining HSPC fate during emergence from the HE. Using time-lapse microscopy, we discovered that in zebrafish *vegfc* loss-of-function embryos there is a decrease in EHT and budding of HSPCs from the DA. We observed more cells crawling along the cardinal vein, which we confirmed were myeloid cells emerging from the DA. Our findings provide insight into fate regulation during EHT that may be useful in guiding *in vitro* differentiation of HSPCs for clinical stem cell therapy.

RESULTS

VEGFC is expressed in HSPCs and HE

Using existing gene expression datasets, we examined *VEGFC* expression in both mouse (*Vegfc*) and zebrafish (*vegfc*) HE and HSPCs. Gene expression analysis of sorted mouse hematopoietic populations showed that *Vegfc* is most highly expressed in undifferentiated HSPCs (Fig. S1A) (Gazit et al., 2013; Seita et al., 2012). Single-cell RNA sequencing (scRNA-seq) of mouse DA from E9.5 to E11.5 showed that *Vegfc* is expressed specifically in a population of pre-HE and HE cells (Fig. S1B,C) (Zhu et al., 2020). In zebrafish, whole-mount *in situ* hybridization (WISH) expression of *vegfc* has been observed in the DA at pre-HE [26 h post fertilization (hpf)] and HE stages (48-72 hpf) (Gore et al., 2011; Kwon et al., 2013).

We wanted to determine the expression of *vegfc* and its receptors in EC and HSPC populations at 52 hpf so we performed scRNA-seq of sorted *flk:mCherry*+ and *cd41:gfp*+ cells, respectively, from *flk:mCherry;cd41:gfp* double transgenic embryos. Using Seurat analysis, we identified 17 unique clusters (Fig. S2). We used *myb* (*cmyb*) and *gata2b* to identify HSPC clusters, *kdrl* (*vegfr2a*) for ECs, and *mpx* for myeloid cells (Fig. S3A,C). As expected, HSPCs express *GFP* transcripts (*cd41:gfp*) and ECs express *mCherry* (*flk:mCherry*) (Fig. S3B). Regarding expression of *vegfc* and its receptors, *kdrl* is expressed in ECs and a few HSPCs, *vegfr3* is expressed only in ECs, and *vegfc* is expressed in ECs and a subset of HSPCs (Fig. S3C). Given the conserved expression of *VEGFC* in both mouse and zebrafish embryonic HSPCs, we wanted to further explore its functional role in HSPC development.

vegfc loss-of-function decreases HSPC emergence from the DA

To determine whether *vegfc* plays a role in definitive hematopoiesis, we used a combination of genetic tools, including *vegfc*^{um18} null mutants (Shin et al., 2016) and a previously validated *vegfc* morpholino (MO) (Villefranc et al., 2013). We also designed a CRISPR-Cas9 single guide RNA (sgRNA) to target *vegfc* in transient F0 crispants. Our sgRNA target showed 97.34% gene editing efficiency and deletions were found around the predicted cleavage site (Fig. S4A-C). We wanted to confirm that crispants and morphants displayed signs of defective lymphangiogenesis and lymphedema consistent with *vegfc*^{um18} null mutants (Shin et al., 2016). To assess lymphedema, we raised *vegfc* MO-injected and crispant-injected embryos until 5 days post fertilization (dpf) and evaluated their overall morphology. Similar to *vegfc*^{um18} null embryos, *vegfc* crispant and morphant embryos had areas of lymphedema that were not seen in control embryos (Fig. S5A,B,E,F). We examined sprouting of parachordal lymphangioblasts (PLs) in *vegfc* crispants and morphants (Fig. S5C,D,G,H) and found they had the same defects that are typical for *vegfc* mutants (Vogrin et al., 2019; Le Guen et al., 2014). We went on to use these validated genetic tools to address the function of *vegfc* in developmental hematopoiesis.

We wanted to examine HSPC formation in *vegfc* loss-of-function embryos. We looked at *cmyb* marker expression by WISH in the DA at 36 hpf and observed significantly lower expression in *vegfc* loss-of-function embryos compared with controls (Fig. S6A,B). Based on these results, we wanted to track the live dynamics of EHT in *vegfc* loss-of-function embryos. Preliminary time-lapse experiments conducted from 32 to 52 hpf revealed that HSPC production is at its highest at 48 hpf (Fig. S6C), which is consistent with previous studies (Kissa et al., 2008; Lancino et al., 2018; Kissa and Herbomel, 2010). Therefore, we performed time-lapse imaging of *flk:mCherry;cd41:gfp* embryos from 48 hpf until 52 hpf. This revealed that *vegfc* loss-of-function embryos had significantly fewer HSPCs budding from the DA (Fig. 1A,B). HSPCs were quantified based on expression of both *flk:mCherry* and *cd41:gfp*, as well as their process of rounding up from the endothelium and budding into the cardinal vein (Fig. 1C; Movie 1). Interestingly, *vegfc* loss-of-function embryos appeared to have more cells that started to extrude from the ventral wall of the DA, as has been previously observed (Kissa and Herbomel, 2010), but they were not able to complete EHT (Fig. 1D; Movie 2). These findings were also confirmed in *vegfc* morphant embryos (Fig. S6D-F). We did not observe defective blood flow in *vegfc* loss-of-function embryos, and circulating cells are always visible (Movies 2, 4, 6, 8). Furthermore, we used the *tp1:dGFP* notch reporter line to confirm that the arterial endothelium is intact in *vegfc* loss-of-function embryos before HSPC formation at 28 hpf (Fig. S6G). These results suggest that *vegfc* plays a role in HSPC emergence but not in earlier vascular patterning or specification of the DA.

vegfc loss-of-function embryos show decreased *cd41:gfp*+ HSPCs in the CHT

After observing a significant decrease in HSPCs in the DA, we wanted to determine whether the effects of *vegfc* loss-of-function are maintained throughout development. After emergence from the DA, HSPCs migrate through circulation to seed the CHT, where they expand in number (Ciau-Uitz et al., 2014; Murayama et al., 2006). Using the HSPC transgenic reporter line *cd41:gfp* we observed significantly fewer *cd41:gfp*+ cells in the CHT of *vegfc* loss-of-function embryos (Fig. 2A,B; Fig. S7A,B). The decrease in *cd41:gfp*+ cell lodgment in the CHT was not due to defective EC pocket formation (Tamplin et al., 2015), as these niche structures were still present in *vegfc* loss-of-function embryos (Fig. S7C,D). Decreased HSPCs were further confirmed using our scRNA-seq datasets from control and *vegfc* loss-of-function *flk:mCherry;cd41:gfp* embryos (Figs S2 and S3). The percentage of cells in the HSPC

Development (2022) 149, dev199498. doi:10.1242/dev.199498

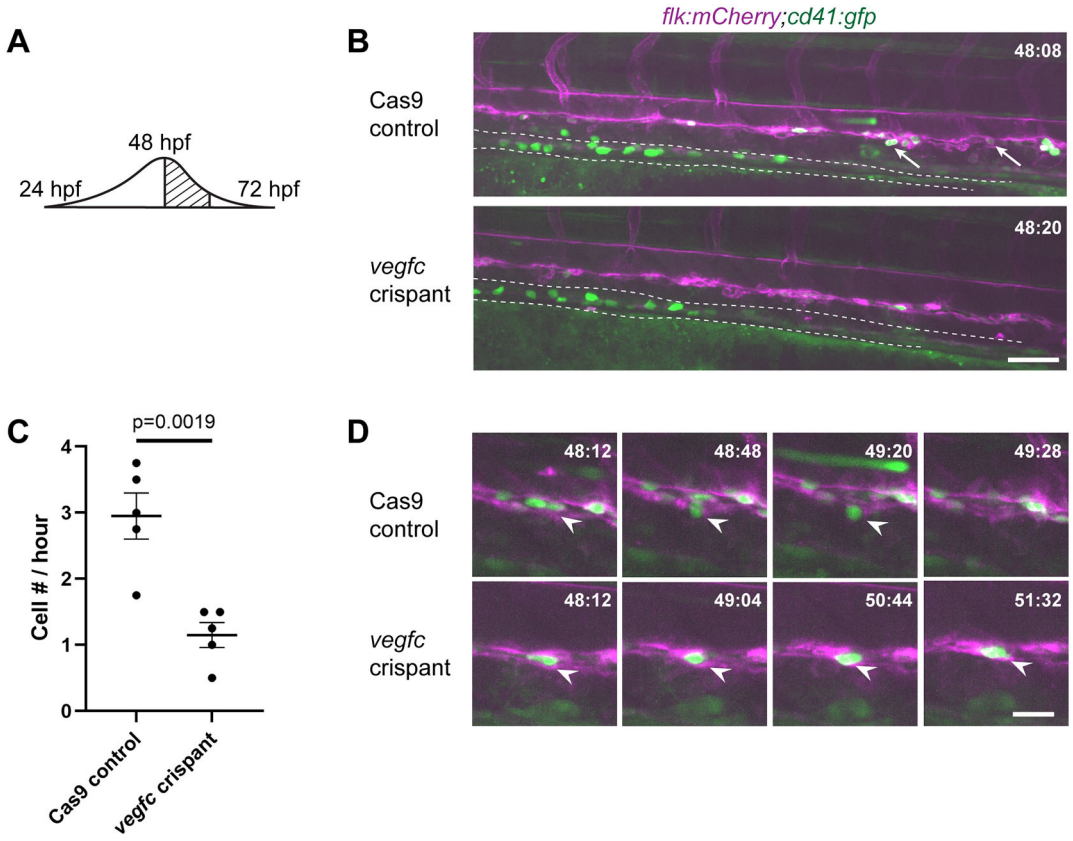

Fig. 1. *vegfc* loss-of-function results in decreased HSPC emergence from the DA. (A) Schematic showing the wave of emergence from the DA; this experiment occurs during the peak. (B) Single frame of time-lapse (hpf:min) showing *cd41:gfp*+ (green) HSPCs (arrows) budding from *flk:mCherry*+ (magenta) HE in Cas9 control (top panel) or *vegfc* crispant embryos (bottom panel). Dotted line outlines developing pronephric tubules (see Movies 1 and 2). (C) Quantification of the total number of *cd41:gfp*+ HSPCs budding from the DA between 48 and 52 hpf, divided by four to give cell number (#) per hour. *n*=5 embryos per condition, *P*=0.0019 (unpaired two-tailed *t*-test). (D) Four frames selected from Cas9 control and *vegfc* crispant time-lapse movies depicting HSPC budding (top panels) and a static hammock-like cell (bottom panels). White arrowheads indicate the cell of interest. Error bars show mean±s.e.m. Scale bars: 50 µm (B); 10 µm (D).

cluster was lower in *vegfc* morphants (5%) compared with controls (12%) (Fig. S2C).

We wanted to determine whether this decrease in HSPC emergence and colonization of the CHT indicated a sustained reduction in definitive hematopoiesis. We assessed *rag1* expression in the 5 dpf thymus, as thymic seeding is dependent on the emergence of definitive HSPCs from the DA (Jin et al., 2007; Murayama et al., 2006). *vegfc* crispant and morphant embryos had significantly lower *rag1* expression than control embryos (Fig. 2C,D; Fig. S7E,F). To further confirm the specificity of our genetic tools, we attempted to rescue definitive hematopoiesis in *vegfc* morphants using a MO-resistant *vegfc* mRNA (Fig. S8A). Co-injection of *vegfc* MO with either 200 or 400 pg of rescue mRNA dose-dependently restored *rag1* expression in the thymus at 5 dpf (Fig. S8B,C). To confirm the specificity of *vegfc* crispants, we co-injected the same *vegfc* MO-resistant mRNA and measured *rag1* expression at 5 dpf. Injection of *vegfc* mRNA was able to restore *vegfc* crispant *rag1* expression to control levels (Fig. S8D,E). Finally, we wanted to determine whether overexpression of *vegfc* would increase HSPC numbers. We injected the same *vegfc* MO-resistant mRNA and quantified *cd41:gfp* cells at 72 hpf, but observed no change (Fig. S8H,I). Together, these data show *vegfc* morphant and crispant phenotypes faithfully recapitulate genetic mutant alleles. Furthermore, loss-of-function embryos show impaired definitive hematopoiesis beginning with reduced HSPC emergence in the DA and persisting through to progenitor seeding of the thymus at 5 dpf.

To further interrogate definitive hematopoiesis in the CHT of *vegfc* loss-of-function embryos, we examined expression of the *cmyb* marker using WISH. Interestingly, in contrast to the decrease of *cd41:gfp*+ cells we observed in the CHT of *vegfc* crispant (Fig. 2A,B) and morphant (Fig. S7A,B) embryos, there were significantly more *cmyb*+ cells in *vegfc* crispants (Fig. 2E,F), *vegfc*^{um18} null (Fig. 2G,H), and *vegfc* morphant embryos (Fig. S7G,H) compared with controls. We performed a rescue experiment in *vegfc* morphants and saw that co-injection of *vegfc* MO and MO-resistant *vegfc* mRNA, but not control mRNA, could rescue *cmyb* expression (Fig. S8F,G). We wanted to resolve opposing results between *cd41:gfp*+ and *cmyb*+ WISH as HSPC markers in the CHT of *vegfc* loss-of-function embryos. Studies in chicken embryos showed that *cmyb* marks myeloid cells in addition to HSPCs (Duprey and Boettiger, 1985). Therefore, we wanted to test the hypothesis that increased *cmyb* expression resulted in part from an increase in myeloid progenitor cells. We used *cmyb:gfp;lyz:DsRed2* embryos to visualize putative *cmyb:gfp*+ HSPCs together with *lyz:DsRed2*+ myeloid cells in the same embryo (Fig. S9A). We found that 55.87%±2.16 (mean±s.e.m.) of cells were *cmyb:gfp*+, 44.12%±2.16 were *lyz:DsRed2*+ and 34.70%±1.79 were double positive (Fig. S9B). We identified HSPCs by their round shape and expression of *cmyb:gfp* alone. We considered myeloid cells as *lyz:DsRed2*+ that were positive or

Development (2022) 149, dev199498. doi:10.1242/dev.199498

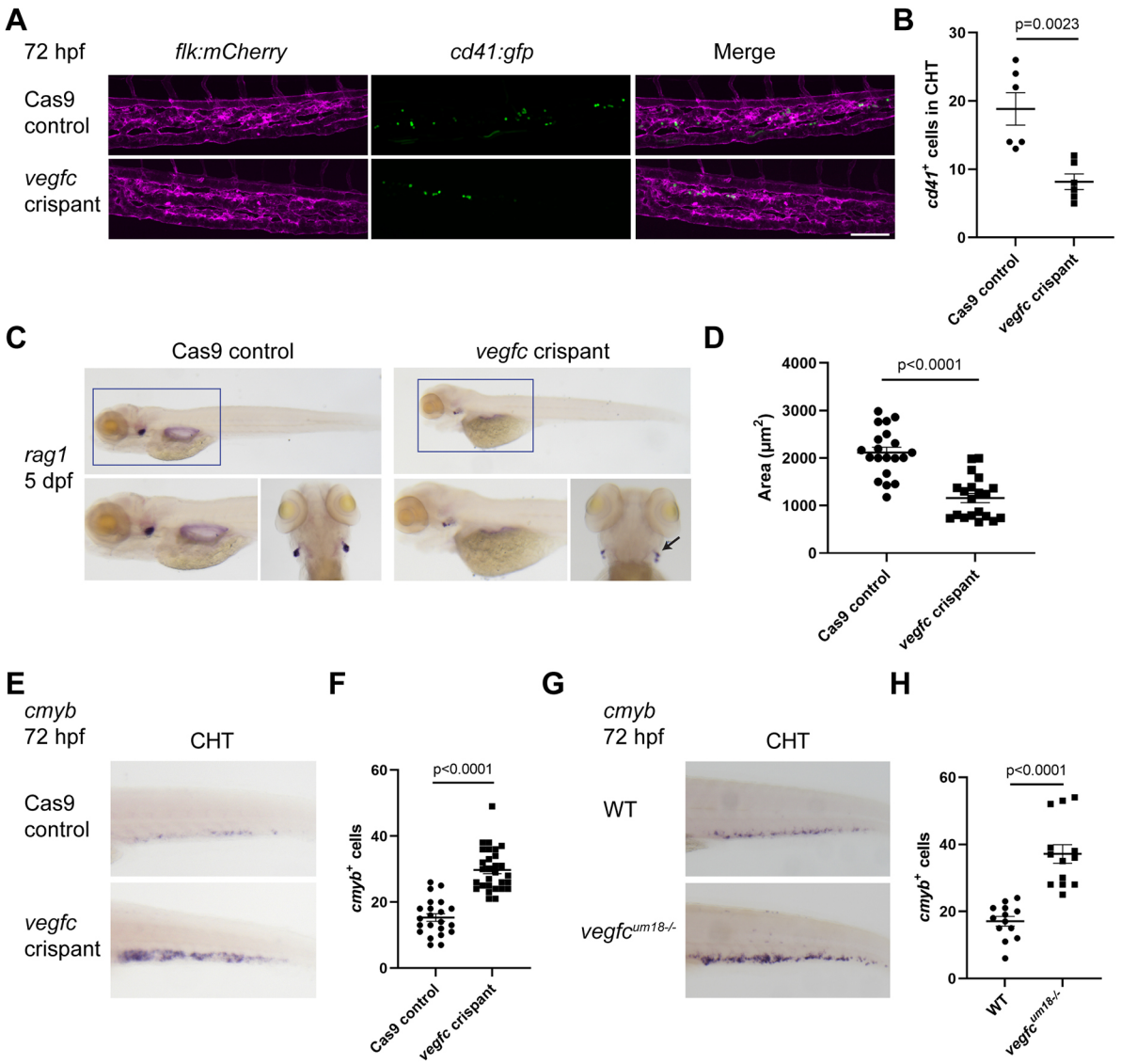

Fig. 2. *vegfc* loss-of-function leads to altered definitive hematopoiesis throughout development. (A) *In vivo* imaging of *cd41:gfp* (green; HSPCs) and *flk:mCherry* (magenta; vessels) depicting decreased HSPC numbers in the CHT of *vegfc* loss-of-function embryos at 72 hpf. (B) Quantification of *cd41:gfp*+ cells within the CHT, as shown in A; Cas9 control versus *vegfc* crispants, P=0.0023 (unpaired two-tailed *t*-test). (C) *vegfc* crispants show decreased area of *rag1* expression in the thymus at 5 dpf. Black arrow highlights area of *rag1* staining in *vegfc* crispant. (D) Quantification of the area of *rag1* expression, P<0.0001 (unpaired two-tailed *t*-test). (E) *vegfc* loss-of-function increases the number of *cmyb*-expressing cells in the CHT compared with Cas9 control embryos. (F) Quantification of the number of *cmyb*-expressing cells in the CHT at 72 hpf, P<0.0001 (unpaired two-tailed *t*-test). (G) *vegfc*$^{um18-/-}$ mutant embryos show an increased number of *cmyb*-expressing cells in the CHT at 72 hpf. (H) Number of *cmyb*-expressing cells in the CHT at 72 hpf, P<0.0001 (unpaired two-tailed *t*-test). Error bars show mean±s.e.m. Scale bar: 40 µm (A).

negative for *cmyb:gfp*. Next, we used *cd41:gfp;lyz:DsRed2* embryos to determine whether the *cd41:gfp* transgenic line also marked myeloid cells in addition to HSPCs (Fig. S9C). We found that 48.13% ±1.96 of cells were *cd41:gfp*+, 51.86%±1.96 were *lyz:DsRed2*$^{+}$ and we found no cells that were double positive (Fig. S9D). These results suggest that *cd41:gfp* is a more specific reporter for HSPCs than *cmyb:gfp*. Furthermore, although *vegfc* loss-of-function embryos have decreased *cd41:gfp*+ HSPC numbers, the increase in *cmyb*+ WISH expression suggests an abundance of myeloid progenitors.

vegfc loss-of-function embryos have an increase in myeloid progenitors

We wanted to further characterize the possible increase in myeloid progenitors upon *vegfc* loss-of-function. First, we examined the myeloid marker *mpx* using WISH and found there was a significant increase in *vegfc* loss-of-function embryos in the CHT at 56 hpf, compared with Cas9 controls (Fig. 3A,B). Genetic mutant *vegfc*^{um18} and *vegfc* morphant embryos also showed an increase in *mpx*+ cells in the CHT at 56 hpf (Fig. 3C, D; Fig. S10A,B). This was consistent with our finding that a proportion of the increased *cmyb*+ cells in *vegfc* loss-of-function embryos are likely myeloid progenitors (Fig. 2E-H; Fig. S7G,H), as suggested by the colocalization of *cmyb:gfp* with myeloid marker *lyz:DsRed2* (Fig. S9A,B). To further confirm increased myeloid marker expression, we used the transgenic line *lyz:DsRed2* to visualize myeloid cells at 72 hpf and saw an increased number of cells in the CHT of *vegfc* loss-of-function embryos (Fig. 3E,F). This was also confirmed using *mpx:gfp*+ cells in *vegfc*

Development (2022) 149, dev199498. doi:10.1242/dev.199498

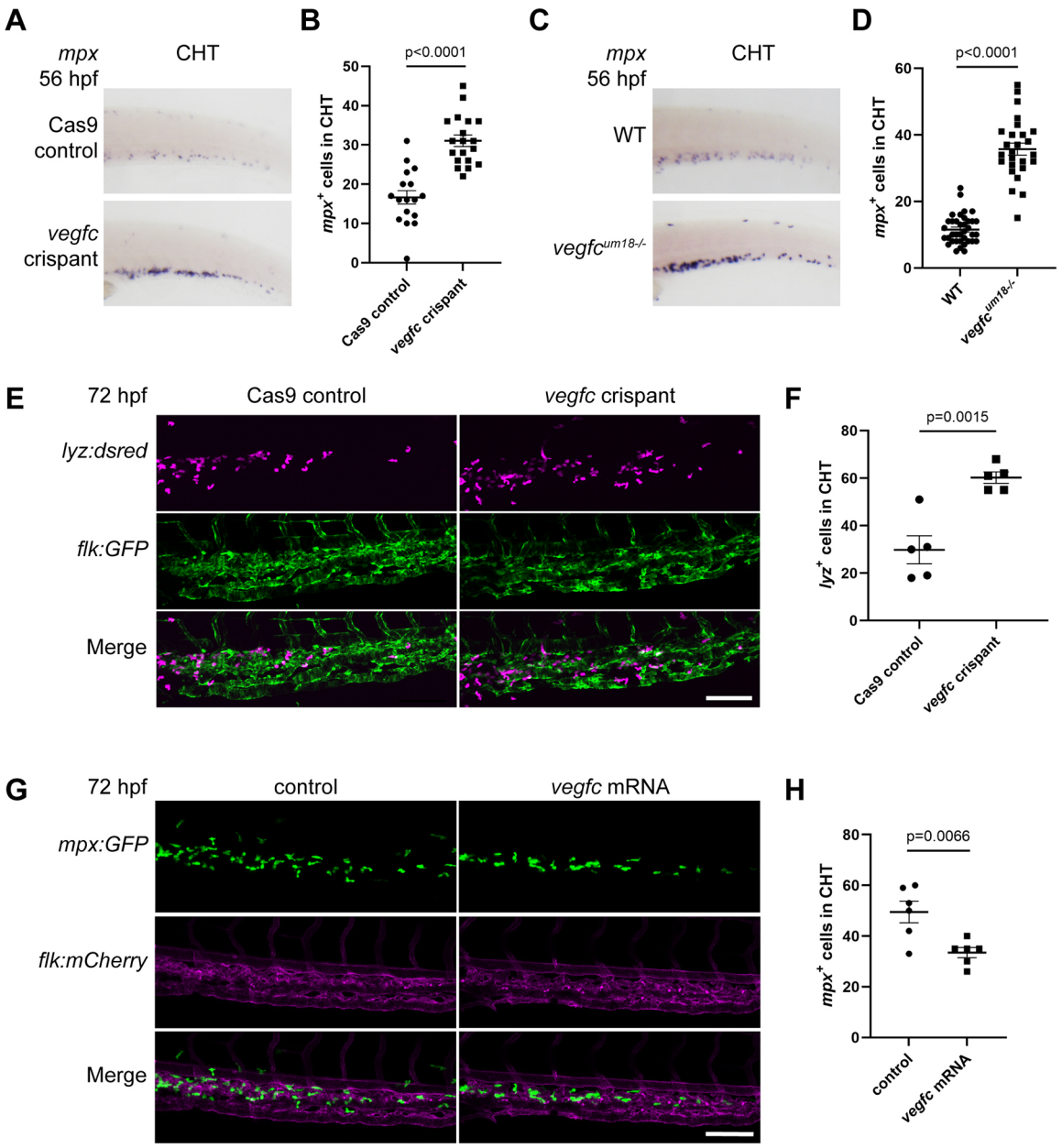

Fig. 3. *vegfc* loss-of-function embryos display an increase in myeloid cells in the CHT. (A) *vegfc* loss-of-function increases the number of *mpx*-expressing cells in the CHT region at 56 hpf. (B) Quantification of the number of *mpx*-expressing cells in the CHT at 56 hpf, $P<0.0001$ (unpaired two-tailed *t*-test). (C) *vegfc*$^{um18-/-}$ mutant embryos show increased *mpx* expression in the CHT at 56 hpf. (D) Quantification of the number of *mpx*-expressing cells in the CHT at 72 hpf, $P<0.0001$ (unpaired two-tailed *t*-test). (E) *vegfc* loss-of-function increases the number of *lyz:DsRed2*+ (magenta) cells in the CHT at 72 hpf. *flk:gfp*+ vessels are green. (F) Quantification of *lyz:DsRed2*+ cells within the CHT, $P=0.0015$ (unpaired two-tailed *t*-test). (G) Overexpression of *vegfc* decreases the number of *mpx:gfp*+ (green) cells in the CHT at 72 hpf. *flk:mCherry*+ vessels are magenta. (H) Quantification of the number of *mpx*-expressing cells in the CHT at 72 hpf, $P=0.0066$ (unpaired two-tailed *t*-test). Error bars show mean±s.e.m. Scale bars: 50 µm (E,G).

morphants (Fig. S10C,D). Increased myeloid cells were further confirmed using our scRNA-seq dataset. The *mpx*+ cluster of myeloid cells (Fig. S2B, cluster #5; Fig. S3A), showed an increase in the total proportion of cells in *vegfc* morphants (7%) compared with controls (3%) (Fig. S2C). We were also interested in how overexpression of *vegfc* would impact myeloid numbers in the CHT. To do this, we injected embryos with the same *vegfc* rescue mRNA described above and quantified the number of *mpx*+ cells in the CHT at 72 hpf. Overexpression of *vegfc* resulted in decreased *mpx*+ cells compared with controls (Fig. 3G,H). The observed increase or decrease in myeloid progenitors with *vegfc* loss-of-function or overexpression, respectively, suggests that *vegfc* could play a role in regulating hematopoietic fate decisions.

We next wanted to determine whether *vegfc* loss-of-function results in an overall myeloid bias, or whether it is specific to neutrophils or macrophages. In order to determine whether neutrophil numbers were impacted, we used Sudan Black B stain, a lipophilic stain that binds to granules in neutrophils (Sheehan and Storey, 1947). Loss of *vegfc* resulted in significantly more stained cells in the CHT than in uninjected controls (Fig. S10E,F). We used the transgenic line *mpeg:gfp* to investigate macrophage numbers in *vegfc* loss-of-function embryos and found a significant increase in

Development (2022) 149, dev199498. doi:10.1242/dev.199498

the CHT (Fig. S10G,H). We saw increased numbers of both CHT neutrophils and macrophages, suggesting that *vegfc* loss-of-function results in an overall increase in myeloid cells.

Neutrophils in *vegfc* loss-of-function embryos have an altered injury response

After observing that *vegfc* loss-of-function embryos have more CHT myeloid cells than control embryos, we wanted to investigate whether they are still functional and able to respond to injury. Caudal fin transection is an *in vivo* injury model of inflammation and wound repair that produces a robust and well-characterized neutrophil response (Isles et al., 2019; Miskolci et al., 2019; Ellett et al., 2015). We transected a portion of the caudal fin at 72 hpf and fixed embryos at 2, 6 and 24 h post injury (hpi) (Fig. 4A). Control embryos showed a typical pattern of response, with the number of neutrophils at the site of injury peaking at 6 hpi (Fig. 4B,D). Embryos with *vegfc* loss-of-function showed an altered timing, with their response peaking at 2 hpi and diminishing over 24 h (Fig. 4C,D). Both treatment groups resolved injury at 24 hpi, with no statistical difference in the number of neutrophils in the wound area (Fig. 4D). The higher number of neutrophils at the injury site of *vegfc* loss-of-function embryos at 2 hpi may be explained by the higher number of available neutrophils in the CHT (Fig. 4E,F), or more rapid migration to the site of injury. Our results demonstrate that the neutrophils in *vegfc* loss-of-function embryos are still able to respond to injury and migrate to the wound site.

vegfc loss-of-function embryos show altered HSPC behavior in the DA

We wanted to determine the origin of increased myeloid cells in *vegfc* loss-of-function embryos. We considered that HE cells failing to undergo EHT in *vegfc* loss-of-function embryos during the peak of emergence (Fig. 1; 48-52 hpf), may persist in the DA until later stages. To resolve this, we performed time-lapse imaging of the DA during a later time window, from 56-72 hpf. During later-stage EHT in control embryos we still observed cells budding from the DA; however, the frequency was reduced from ∼3 per hour at 48-52 hpf to less than one per hour at 56-72 hpf (compare Figs 1C and 5C; Fig. S11C). Although there was no significant difference in the number of budding cells between control and *vegfc* loss-of-function

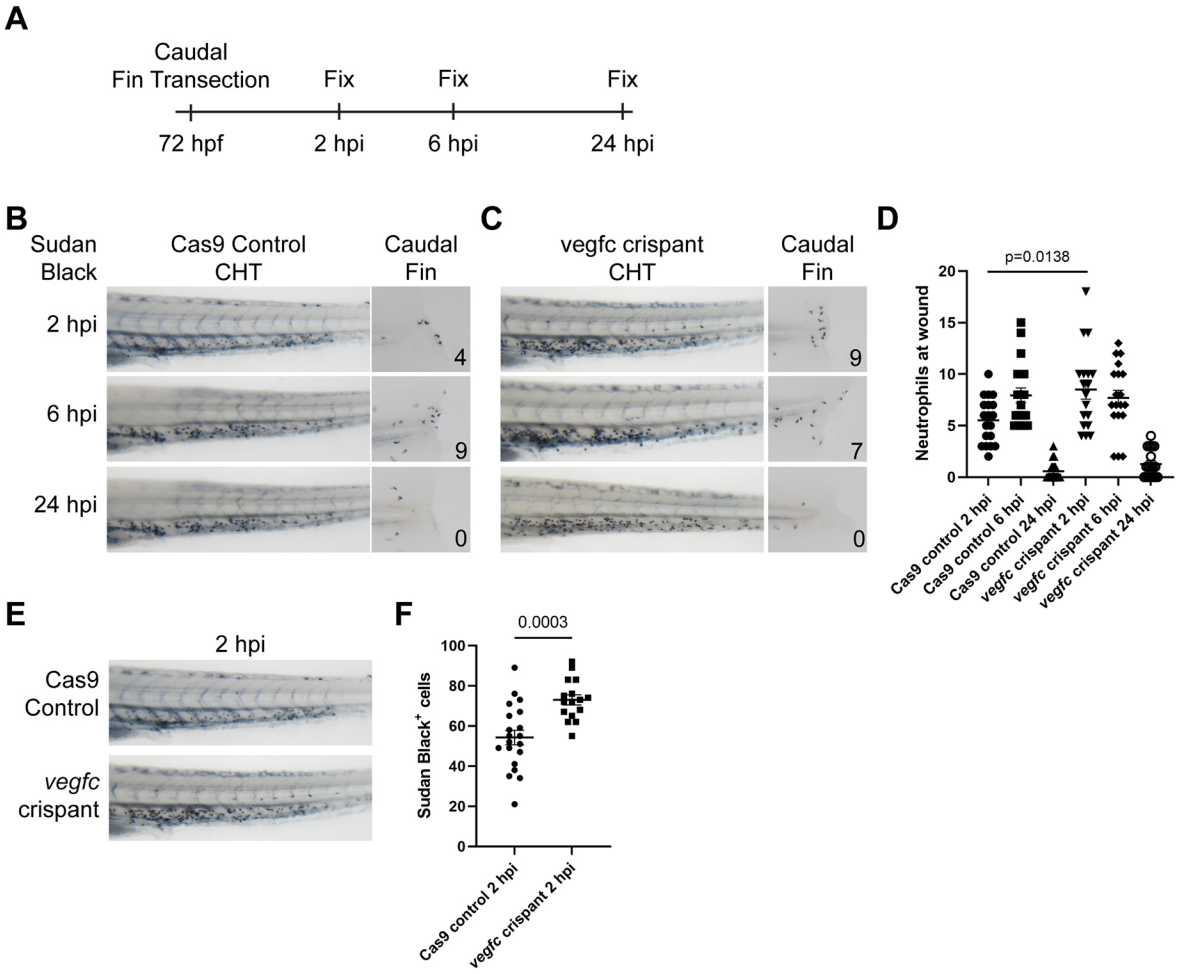

Fig. 4. *vegfc* loss-of-function embryos show altered injury response. (A) Experimental approach. Caudal fins were transected distally without injury of the notochord at 72 hpf. Embryos were fixed in 4% PFA at different intervals following transection. (B) Bright-view images of Sudan Black staining in Cas9 control embryos depicting neutrophil response at 2, 6 and 24 hpi. Neutrophil response peaks at 6 hpi and subsides by 24 hpi. (C) Bright-view images of Sudan Black staining in *vegfc* loss-of-function embryos. Neutrophil response peaks at 2 hpi and diminishes over time. (D) Quantification of neutrophil number within the injury area, P=0.0138 (comparison between Cas9 control 2 hpi and *vegfc* crispant 2 hpi; one-way ANOVA). (E) Representative images showing increased neutrophils within the CHT of *vegfc* loss-of-function embryos at 2 hpi. (F) Quantification of the number of Sudan Black-positive neutrophils within the CHT at 2 hpi, P=0.0003 (unpaired two-tailed *t*-test). Error bars show mean±s.e.m.

Development (2022) 149, dev199498. doi:10.1242/dev.199498

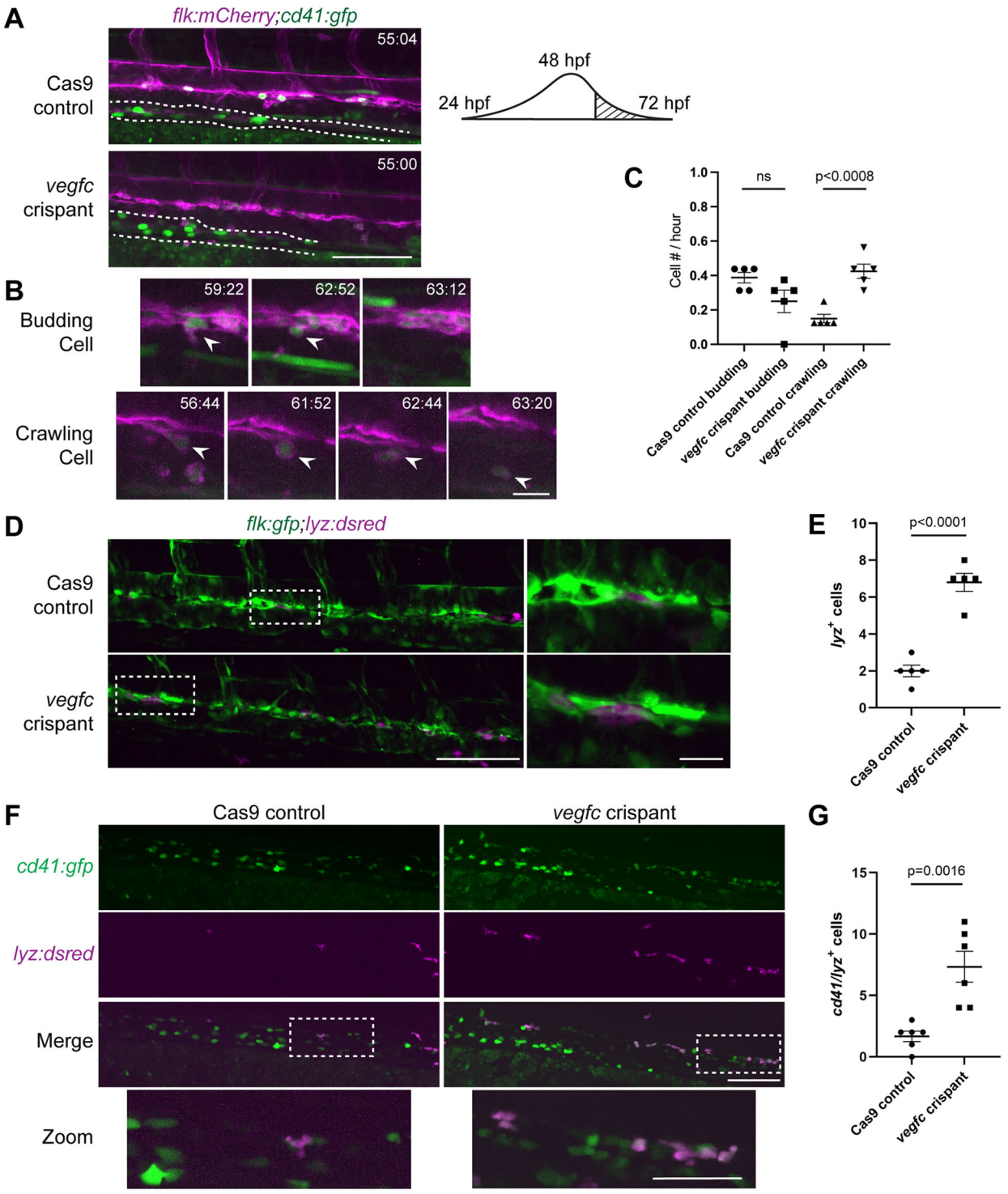

Fig. 5. Late-stage hemogenic endothelium in *vegfc* loss-of-function embryos gives rise to increased crawling myeloid-like cells. (A) Single frames of *cd41:gfp*+ (green) and *flk:mCherry*+ (magenta) time-lapse (hpf:min) showing the overall difference in DA morphology between Cas9 controls (top panel) and *vegfc* crispants (bottom panel). The dotted line outlines the pronephric tubules. Right shows a schematic showing the time window of imaging for this experiment that is past the peak of HSPC emergence form the DA. (B) Three frames selected from Cas9 control time-lapse movie (Movie 3) between 56-72 hpf depicting HSPC budding (top). Four frames selected from *vegfc* crispant time-lapse movie (Movie 4) depicting HSPC crawling (bottom). White arrowheads indicate the cell of interest. (C) Quantification of *cd41:gfp*+/*flk:mCherry*+ cell behavior within the DA, $P<0.0008$ (control versus crispant, budding or crawling; one-way ANOVA). The total number of events observed are divided by the duration of the experiment (16 h) to give the number of events per hour. The data shown is from one experiment with a total of $n=5$ control and $n=5$ *vegfc* crispant embryos. (D) Single frames of *flk:gfp*+/*lyz:DsRed2*+ time-lapse (hpf:min) showing the overall number of *lyz:DsRed2*+ cells within the DA of Cas9 controls (top panel) and *vegfc* crispants (bottom panel). Right panels show magnification of boxed areas on left. (E) Quantification of the number of resident *lyz:DsRed2*$^+$ cells within the ventral wall of the DA, $P<0.0001$ (unpaired two-tailed *t*-test). (F) *vegfc* crispants show increased *cd41:gfp*+/*lyz:DsRed2*+ cells in the DA at 56 hpf. Bottom panel shows magnified image of double-positive cells (boxed area above). (G) Quantification of the number of *cd41:gfp*+/*lyz:DsRed2*+ cells within the DA, $P=0.0016$ (unpaired two-tailed *t*-test). Error bars show mean±s.e.m. Scale bars: 40 µm (A); 10 µm (B, D magnification); 100 µm (D,F); 50 µm (F magnification).

Development (2022) 149, dev199498. doi:10.1242/dev.199498

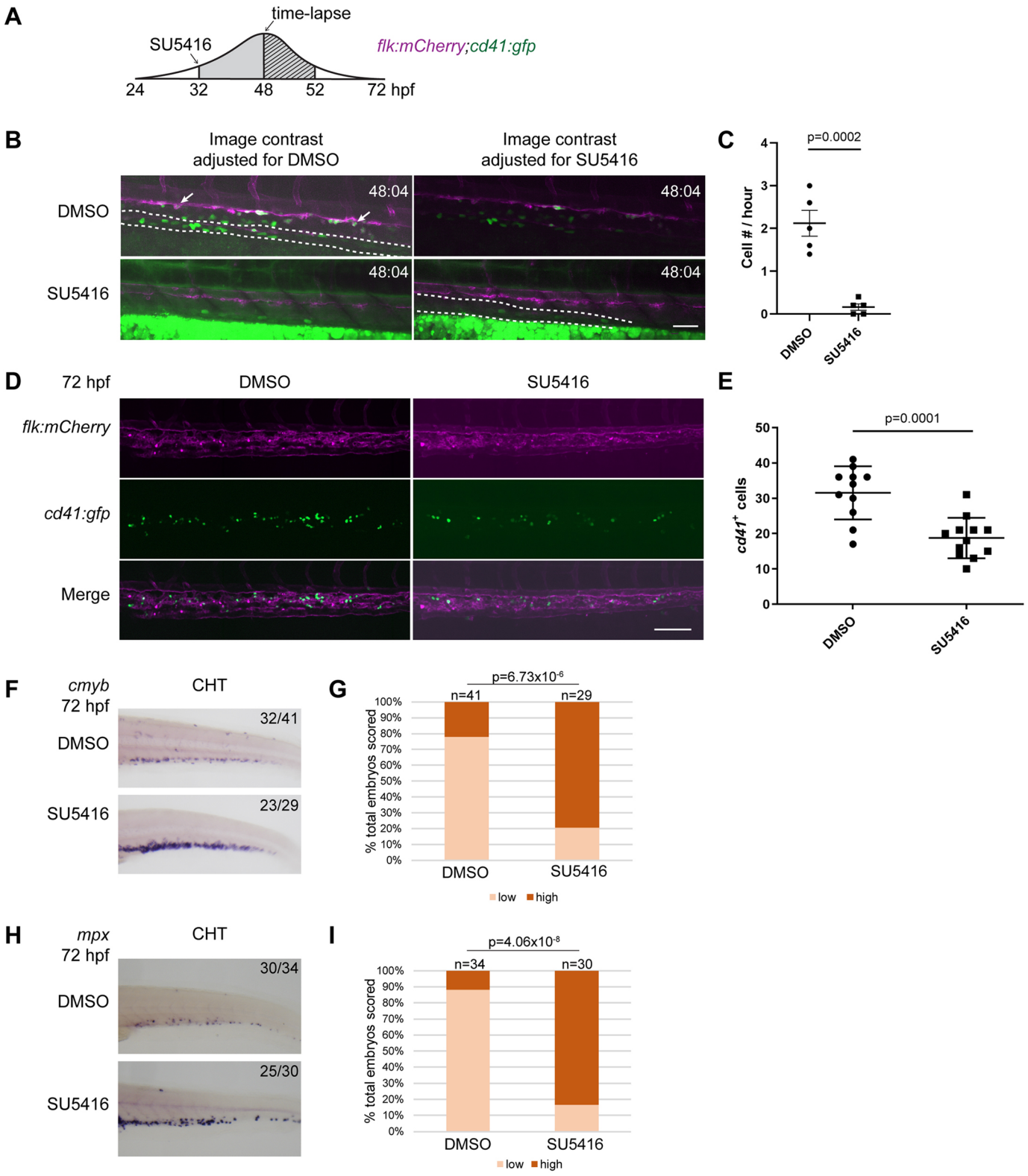

Fig. 6. See next page for legend.

embryos from 56-72 hpf, we did observe a significant increase in the number of cells that exhibited crawling behavior in *vegfc* loss-of-function embryos (Fig. 5A-C; Fig. S11A-C; Movies 3 and 4). Comparison of late stage HE shows very different morphology between control and *vegfc* loss-of-function embryos, with the latter showing increased *cd41:gfp+* cell movement and altered cell morphology. Time-lapse imaging showed that *vegfc* loss-of-function resulted in cells of the ventral wall of the DA extending filopodia and crawling around the cardinal vein, instead of rounding up and budding off into circulation as in controls (Fig. 5A,B;

Development (2022) 149, dev199498. doi:10.1242/dev.199498

Fig. 6. Chemical inhibition of Vegf family receptors phenocopies *vegfc* loss-of-function. (A) Experimental schematic showing SU5416 dosage starting at 32 hpf, followed by time-lapse imaging from 48 to 52 hpf. The hatched area indicates the time-lapse window, and the gray area indicates the time of SU5416 treatment. (B) Treatment of embryos with SU5416 created high levels of autofluorescence in the yolk sac. Therefore, we present images with levels (brightness and contrast) optimized for GFP signal in DMSO-treated control embryos (left column) and SU5416-treated embryos (right column). Single frames of the time-lapse (hpf:min) show *cd41:gfp*+ HSPCs (green) budding from the *flk:mCherry*+ DA (magenta) (Movie 9). White arrows indicate cells undergoing EHT. Compared with DMSO controls (top panels), there are very few budding HSPCs in SU5416-treated embryos (bottom panels) (Movie 10). Dotted lines outline pronephric tubules. (C) Quantification of the total number of *cd41:gfp*+ HSPCs budding from the DA between 48 and 52 hpf. The total number of events observed are divided by the duration of the experiment (4 h) to give the number of events per hour. The data shown is from one experiment with n=5 DMSO- and n=5 SU5416-treated embryos. P=0.0002 (unpaired two-tailed t-test). (D) *In vivo* imaging of the CHT in *cd41:gfp/flk:mCherry* embryos at 72 hpf, after treatment with SU5416 from 32 hpf, shows a reduction in HSPC numbers. (E) Quantification of *cd41:gfp*+ cells within the CHT, as shown in D; DMSO control (n=11) versus SU5416-treated (n=12). P=0.0001 (unpaired two-tailed t-test). (F) Treatment with SU5416 increases the percentage of embryos with high *cmyb* expression compared with DMSO-treated embryos. *cmyb* expression was scored in the CHT at 72 hpf. (G) Percentage of total embryos scored and classified as having low or high *cmyb* expression, $P=6.73\times10^{-6}$ (chi-square goodness of fit test). (H) Treatment with SU5416 increases the percentage of embryos with high *mpx* expression compared with DMSO controls. (I) Percentage of total embryos scored and classified as having low or high *mpx* expression, $P=4.06\times10^{-8}$ (chi-square goodness of fit test). SU5416 dose is 0.75 µM in DMSO. Scale bars: 50 µm (B,D).

Fig. S11A,B; Movies 3 and 4). Crawling cells appear to have decreased *cd41:gfp* intensity compared with budding HSPCs that we hypothesize have downregulated the HSPC-specific *cd41* promoter as they differentiate towards a myeloid fate. *vegfc* loss-of-function embryos showed a significant increase in *flk:mCherry+;cd41:gfp*+ HE cells that were crawling out of the DA and around the CV (Fig. 5C; Fig. S11C). The number of *flk:mCherry*$^{+}$*;cd41:gfp*+ budding cells was not significantly different (Fig. 5C; Fig. S11C).

We wanted to find whether the increase in crawling cells in the DA was consistent with an increase in myeloid progenitors. We performed time-lapse imaging of *lyz:DsRed2;flk:gfp* embryos from 54-72 hpf and quantified the number of *lyz:DsRed2*+ cells residing in the DA. In *vegfc* loss-of-function embryos we saw significantly more *lyz:DsRed2*+ crawling cells in the ventral wall of the DA compared with Cas9 controls (Fig. 5D,E; Movies 5, 6). To further confirm the identity of *lyz:DsRed2*+ cells in the DA, we performed a co-localization experiment with *cd41:gfp*. Cells that resided within the DA were double positive for *lyz:DsRed2;cd41:gfp* and there was a higher number of these cells in *vegfc* loss-of-function embryos compared with controls (Fig. 5F,G; Movies 7,8). To further validate the presence of these putative myeloid progenitors in the HE, we examined expression of *mpx* at 56 hpf. The majority of *vegfc* loss-of-function embryos expressed *mpx* in the DA (>60%), compared with very few control embryos (<10%; Fig. S11D,E). These results suggest that the abundance of myeloid cells in *vegfc* loss-of-function embryos originate from an altered fate in the DA.

Inhibition of Vegf family receptors phenocopies *vegfc* loss-of-function

We wanted to gain insight into the receptors that mediate Vegfc signal in the HE. Recent zebrafish studies showed that Vegfr3 and Kdr, but not Kdrl, are Vegfc targets (Vogrin et al., 2019). We examined *cmyb* expression in the CHT of *vegfr3* mutants at 72 hpf but did not see any difference in expression (Fig. S12). These data, together with published expression data showing that *vegfr3* is expressed in the cardinal vein and not the DA (Gore et al., 2011), suggest that Vegfr3 is not the key receptor for Vegfc signaling in the DA. Next, we treated embryos with the pan-Vegf receptor inhibitor SU5416 (Sukbuntherng et al., 2001; Serbedzija et al., 1999). There is an early requirement for Vegf receptors in patterning the vasculature and DA, and therefore the HE itself, so we started SU5416 treatments later at 32 hpf (Fig. 6A). Next, we performed time-lapse live imaging from 48 to 52 hpf of multiple *flk:mCherry/cd41:gfp* embryos in parallel that were vehicle- or SU5416-treated (Movies 9,10). The number of HSPCs that emerged from the DA was significantly reduced in SU5416-treated embryos (Fig. 6B,C). We did not see any vascular defects or disrupted blood flow in SU5416-treated embryos (Fig. 6B; Movie 10). Consistent with reduced HSPC production from the DA, we observed fewer *cd41:gfp*+ cells in the CHT later at 72 hpf (Fig. 6D,E). Similar to *vegfc* loss-of-function embryos, SU5416-treated embryos also had increased expression of *cmyb* (compare Fig. 6F,G and Fig. 2E-H) and *mpx* (compare Fig. 6H,I and Fig. 3A-D) using WISH at 72 hpf. The comparable decrease in *cd41:gfp*+ HSPCs and increase in *mpx*+ myeloid progenitors, in both *vegfc* loss-of-function and SU5416-treated embryos, suggests that the Vegfc-Vegf receptor signaling axis plays a role in HE fate decisions and the emergence of HSPCs.

DISCUSSION

Many studies have investigated the mechanics of HSPC emergence from the HE, but it is unclear what factors maintain HSPC fate and prevent premature differentiation. Our goal was to investigate the potential role of VEGFC in maintaining HSPC fate, based on its expression within the DA and undifferentiated HSPCs. Currently, the majority of VEGFC studies have detailed its role in lymphangiogenesis (Karkkainen et al., 2004; Küchler et al., 2006; Jeltsch et al., 1997). A few studies in mice have examined the role of VEGFC in hematopoiesis (Hamada et al., 2000; Fang et al., 2016, 2020). In our study, we provide evidence in zebrafish that Vegfc plays a role in regulating HSPC fate decisions during emergence from the DA.

In zebrafish it is thought that HE specification begins with pre-HE cells that contact the somites, before the DA is formed (Clements et al., 2011; Kobayashi et al., 2014). This physical contact is crucial for notch signaling and subsequent specification of HE cells. Loss-of-function of somite-mesoderm cell adhesion factors decreases HSPC numbers (Kobayashi et al., 2014). In chick and mouse, once the DA is formed, the action of mesenchymal-derived VEGF on VEGFR2 acts as a pro-hematopoietic ventralizing factor (Pardanaud and Dieterlen-Lièvre, 1999; Peeters et al., 2009). In studies by Hamada et al. that used P-Sp explants, addition of exogenous VEGFC to wild-type explants suppressed hematopoiesis (Hamada et al., 2000). In the mouse embryo there is likely complex synergism between VEGF and VEGFC as they both bind VEGFR2 and VEGFR3 to regulate early vascular and hematopoietic development (Hamada et al., 2000). In zebrafish, Vegfc is thought to bind Vegfr3 and Kdr, but not Kdrl (Vogrin et al., 2019). Our results would suggest a role for Vegfc after specification of the HE to maintain HSPC fate throughout the full duration of EHT.

In our study, we have shown that embryos lacking *vegfc* have decreased emergence of HSPCs from the HE. The process of HSPC specification appears to be intact in *vegfc* loss-of-function embryos, as *cd41:gfp*+ cells are still present within the HE and a small number of HSPCs are still produced. However, many of these HE cells do not complete EHT, as the exiting cell appears stuck in the ventral

Development (2022) 149, dev199498. doi:10.1242/dev.199498

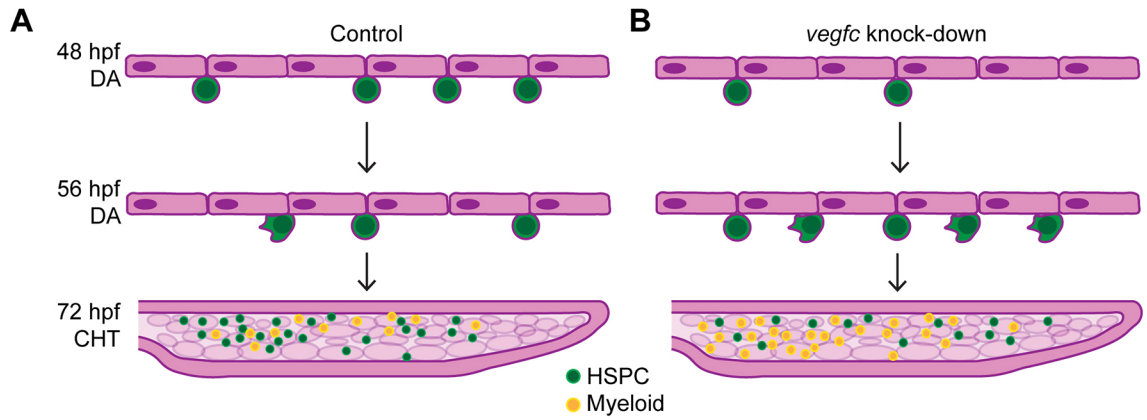

Fig. 7. Model of Vegfc function in determining HE fate decisions in the DA. (A) Schematic of HSPC development in control embryos. Emergence of nascent HSPCs from the DA peaks at 48 hpf. In late stage EHT (56 hpf and later) there is a decrease in HSPC emergence and the appearance of few crawling cells. HSPCs then colonize the CHT, where there are also myeloid cells present. (B) Schematic of HSPC development in *vegfc* loss-of-function embryos. There are significantly fewer HSPCs during the peak of emergence from the DA. In late stage EHT there is a change in cell behavior and many crawling cells emerge from the DA. In the CHT there are decreased HSPCs and an increased number of myeloid cells.

wall of the DA. Normally during EHT, the neighboring rostral and caudal ECs join to maintain continuity in the ventral wall of the DA and aid in HSPC release (Kissa and Herbomel, 2010). This joining of ECs does not appear to occur in *vegfc* loss-of-function embryos, perhaps because they lack the mechanical organization of actin that is required for cell emergence (Lancino et al., 2018). The reduced number of definitive HSPCs persists until larval stages, suggesting that emergent HSPCs stuck in the DA do not recover.

Although *vegfc* loss-of-function embryos have fewer HSPCs, they have a greater number of myeloid progenitors that emerge later from the DA and populate the CHT. We used a caudal fin transection injury model to determine whether *vegfc* loss-of-function embryos produced functional neutrophils (Isles et al., 2019; Ellett et al., 2015). After injury, neutrophil wound response typically peaks at around 6 hpi (Miskolci et al., 2019; Li et al., 2012). In control embryos, we saw the expected peak at 6 hpi; however, injured *vegfc* loss-of-function embryos exhibited a neutrophil wound response that peaked earlier, at 2 hpi. The specific reason for this altered wound response timing is still not clear; however, the neutrophils were still functional in their migration to the site of injury. We speculate that their altered response pattern is due to either faster migration or an increased number of neutrophils in the CHT that are ready to respond to injury.

vegfc loss-of-function embryos show an overproduction of myeloid progenitors that appears to originate from HE. There are a small number of myeloid progenitor cells that normally emerge from the DA (Jin et al., 2009), and these crawling cells are visible in previously published time-lapse live imaging datasets (Lancino et al., 2018; Bertrand et al., 2010). In *vegfc* loss-of-function embryos there are significantly more of these crawling myeloid progenitors produced by the DA. Alternate fates produced from HE of the mouse have been identified, as there are HE-derived HSC precursors that display a B-1 lymphoid bias and go on to differentiate to multipotent progenitors in the FL (Kobayashi et al., 2019). The increase of both *lyz:DsRed2*+ cells and *mpx* expression in the DA of *vegfc* loss-of-function embryos suggests that *vegfc* is involved in regulating HE fate decisions in late-stage DA.

In summary, we propose that VEGFC plays a role in maintaining HSPC fate during emergence from the DA. Based on scRNA-seq of mouse cells from endothelium to HSPCs, *Vegfc* is most highly expressed in pre-HE cells (Zhu et al., 2020). In zebrafish, HSPC emergence from the DA peaks at 48 hpf and then decreases by 56 hpf (Fig. S6C), and there are few myeloid-like crawling cells that emerge. This output is reflected in the CHT, with similar numbers of HSPCs and myeloid cells (Fig. 7A). However, with *vegfc* loss-of-function there are fewer HSPCs produced during the peak of emergence, and by 56 hpf there are many myeloid-like crawling cells that emerge from the DA. In these embryos, the CHT has an overwhelming dominance of myeloid cells, with few HSPCs (Fig. 7B). Our model supports a novel role for VEGFC in maintaining HSPC fate in the HE. A better understanding of the factors that regulate HE development are crucial for optimizing *in vitro* differentiation of pluripotent stem cells into HSPCs (Slukvin, 2013; Ditadi et al., 2017). The ability to promote HSPC versus myeloid fate *in vitro* using VEGFC may have the potential to improve pluripotent stem cell differentiation protocols.

MATERIALS AND METHODS

Fish care

Zebrafish were maintained at the University of Illinois at Chicago (IL, USA) and University of Wisconsin-Madison (WI, USA) in accordance with their respective Institutional Animal Care and Use Committee guidelines. Zebrafish were mated, staged and raised as previously described (Westerfield, 2000). Adult wild-type (AB strain), *vegfc*^{um18} mutants (Villefranc et al., 2013), and the following transgenic lines were used in this study: *Tg(cd41:gfp)* [also known as *la2Tg* or *Tg(-6.0itga2b:eGFP)*] (Lin et al., 2005); *Tg(flk:mCherry)* [*s896Tg* or *Tg(flk1:ras-cherry)*] (Chi et al., 2008); *Tg(mpx:gfp)* [*uwm1Tg* or *Tg(mpx:GFP)uwm1*] (Mathias et al., 2006); *Tg(lyz:DsRed2)* [*nz50Tg* or *Tg(lysC:DsRed2)nz50*] (Hall et al., 2007); *Tg(cmyb:gfp)* [*zf169Tg* or *Tg(cmyb:GFP)unspecified*] (North et al., 2007); *Tg(mpeg:gfp)* [*gl22Tg* or *Tg(mpeg1:EGFP)gl22*] (Ellett et al., 2011); *Tg(tp1:dGFP)* [*Tg(EPV.Tp1-Mmu.Hbb:Venus-Mmu.Odc1)*] (Ninov et al., 2012). *vegfc*^{um18} mutant carriers were genotyped by PCR amplification and Sanger sequencing.

Microinjections of zebrafish embryos

MO targeting the *vegfc* start codon ATG MO, 5′-GAAAATCCAAATAAGTGCATTTTAG-3′ was purchased from GeneTools (Ober et al., 2004). Standard control MO targeting a human β-globin intron mutation, 5′-CCTCTTACCTCAGTTACAATTTATA-3′ was purchased from GeneTools. MO stock solutions were prepared at 1 mM and heated for 10 min at 65°C before preparing injection mix to ensure a uniform solution. Embryos were injected with 4 ng of MO at the one-cell stage and

Development (2022) 149, dev199498. doi:10.1242/dev.199498

compared with uninjected sibling controls. Rescue *vegfc* mRNA was designed to be MO resistant so that the third base pair of each codon was altered to inhibit MO binding but preserve amino acid sequence. The gene sequence was ordered from Genscript and linearized using the *NotI* restriction enzyme (New England Biolabs). mRNA was transcribed using an mMessage mMachine SP6 kit (Invitrogen). *vegfc* MO (4 ng/nl) and rescue mRNA (200 pg/nl or 400 pg/nl) was injected sequentially at the one-cell stage. *Tol2* mRNA at the same concentration as rescue mRNA was used as a negative control.

WISH

Embryos were stage matched and fixed overnight at 4°C in 4% paraformaldehyde (PFA). WISH was performed as previously described (Thisse and Thisse, 2008) with the following exceptions: before permeabilization with proteinase K, embryos were bleached to remove pigmentation and 0.2% glutaraldehyde was added to 4% formaldehyde at the post-fixation step. Antisense RNA probes *cmyb* (Liao et al., 1998), *mpx* (Lieschke et al., 2001) and *rag1* (Willett et al., 1997) were used as previously described. WISH images were quantified using the Cell Counter or Measure features of Fiji/ImageJ. Differential interference contrast microscopy (DIC) images were obtained as described below.

Cell preparation for scRNA-seq

Whole 52 hpf *flk:mCherry/cd41:gfp*+ embryos were dissociated into a single-cell suspension for fluorescence activated cell sorting (FACS) as previously described (Bresciani et al., 2018) with the following exceptions: an additional filter step was added before centrifugation in step 2.3 and final resuspension of single cells was done in PBS+2% fetal bovine serum. The control sample comprised 4000 each of uninjected *flk:mCherry*+ and *cd41:gfp*+ cells, and the *vegfc* MO sample comprised 4000 each of *vegfc* MO *flk:mCherry*+ and *cd41:gfp*+ cells. Then single-cell suspensions were loaded on a Chromium Single Cell Controller (10x Genomics) to generate single-cell gel beads in emulsion (GEMs) by using Single Cell 3′ Library and Gel Bead Kit V3.1 (10x Genomics, 1000121). Cell lysis and RNA barcoding were accomplished through reverse transcription in individual GEMs. Barcoded cDNAs were pooled and cleaned up using SPRIselect beads (Beckman Coulter, B23317). scRNA-seq libraries were prepared using Single Cell 3′ v3.1 Reagents Module 2 (10x Genomics, 1000121) following the manufacturer's instructions. Sequencing was performed on an Illumina NovaSeq 6000 with paired-end 150 bp reads (PE150).

scRNA-seq analysis

CellRanger (5.0.0) was used to generate gene expression containing a unique molecular identifiers (UMIs) matrix using the default parameters. We used a custom zebrafish reference genome (custom_GRCz11_reporters) that included the transgenes EGFP and mCherry. Samples were then further filtered and clustered in Seurat (Stuart et al., 2019). Cells with a feature count between 200 and 3500 and a mitochondrial gene percentage less than 18% were used in analysis, resulting in 5655 high quality single cells. Then, we selected the 2000 most variable genes and fed into Seurat for dimension reduction by principal component analysis (PCA). We ran 'RunPCA' to identify significant principal components (PCs). The top 10 PCs were selected for t-SNE clustering. The 'FindClusters' function was run to find the cell clusters at 0.5 resolution. Cluster identity was assigned manually using known marker genes.

sgRNA design and synthesis

CCTop, E-Crisp and CHOPCHOP were used to identify sgRNA sequences with high on-target activity. Sequence specificity was then confirmed using IDTs software to predict sgRNAs with highest on-target and lowest off-target activities. We chose the following sequence in exon 2 of *vegfc*: GGATAGTTTACCCTACCTAC Pam: CGG. sgRNA was purchased from IDT for the generation of F0 crispants. Primers: forward 5′-ACACTCTTTCCCTACACGACGCTCTTCCGATCTagcatcaaaatctcttgg-ctgt-3′; reverse 5′-GTGACTGGAGTTCAGACGTGTGCTCTTCCGAT-CTgtcaatgttagtatggggcaca-3′. Lowercase letters indicate primer sequences that are specific to the *vegfc* locus and span a 374 bp region covering the sgRNA target region. Uppercase letters show Illumina 5′-3′ Multiplexing Read 1 and 2 adapter sequences, respectively. RNP was assembled and injected as previously described (Burger et al., 2016). We assessed mutagenesis of our sgRNA sequence by extracting genomic DNA from a minimum of 15 embryos and performing Illumina MiSeq sequencing. We then used CRISPResso2 to align and compare the reads (Clement et al., 2019).

Sudan Black staining

Embryos were fixed overnight at 4°C in 4% PFA. Sudan Black stain was performed as previously described (Rosowski et al., 2018). DIC images were obtained as described below.

Imaging

Transgenic zebrafish lines were crossed, and staged embryos were selected by fluorescence microscopy. Embryos were anesthetized in 0.04% tricaine and mounted for live imaging in glass-bottomed dishes or multi-well plates in 1% low-melt agarose and covered with E3 media and tricaine as previously described (Bertrand et al., 2010). The zebrafish embryos were maintained at 28.5°C in an incubated stage. Live time-lapse microscopy was performed using a Zeiss Spinning Disk Confocal using a 20× Plan-Apochromat objective or a Nikon Yokogawa CSU-W1 Spinning Disk Confocal using a 20× objective. Time points were recorded every 3-4 min for the stated time period. WISH and Sudan Black-stained embryos were mounted in 70% glycerol and imaged on a Nikon SMZ18 stereoscope at 4× for whole embryo images and 8x for regional imaging. All confocal images shown are maximum projection in *z*.

Image analysis

Images were processed and analyzed using Zen (Zeiss), Elements (Nikon), Imaris (Bitplane) and Fiji/ImageJ. Confocal *z*-stack images are presented as maximum projections. Cell tracking and counting was performed using the Imaris spot detection feature. For cell behavior quantification, DA-derived *flk:mCherry/cd41:gfp* double-positive cells were quantified based on behavior and classified as either budding or crawling. To be classified as crawling, cells must extend filopodia and move contrary to blood flow in the caudal vein; to be classified as budding, cells must emerge and immediately enter circulation.

Drug treatments

SU5416 (Cayman Chemical, 13342) was dissolved in DMSO and stored at −20°C. Embryos were treated from 32 hpf until 72 hpf with 0.75 µM SU5416, and 0.1% DMSO alone was used as a control. All treatments were diluted in E3 medium.

Statistical analysis

Statistical analysis was carried out using Graph Pad Prism V7.0 or R Studio 1.2. Data are presented as mean±s.e.m. Analysis of two experimental groups was carried out using an unpaired two-tailed Student's *t*-test. Analysis of more than two experimental groups was carried out using one-way ANOVA, with multiple comparisons. Low/high expression analysis of WISH experiments was carried out in R Studio using a chi-square goodness of fit test. *P*-values are indicated in the figures.

Acknowledgements

We thank Dr Nathan Lawson for sharing the *vegfc*^{um18} zebrafish line and Dr Teresa Bowman for sharing the *mpx:gfp*, *cmyb:gfp* and *lyz:DsRed2* transgenic zebrafish lines. Microscopy was performed at The University of Illinois at Chicago RRC Fluorescence Imaging Core and The University of Wisconsin-Madison Optical Imaging Core. Sequencing of genetic mutants was performed at The University of Illinois at Chicago RRC Genome Research Core. We acknowledge the University of Wisconsin-Madison Biotechnology Center Gene Expression Center, DNA Sequencing Facility and Bioinformatics Resource Center for providing scRNA-seq library preparation, next generation sequencing services and data analysis. We acknowledge the University of Wisconsin Carbone Cancer Center Support Grant P30 CA014520 for the Flow Cytometry Laboratory.

Competing interests
The authors declare no competing or financial interests.

Author contributions
Conceptualization: R.K.S., O.J.T.; Methodology: R.K.S., O.J.T.; Validation: R.K.S.; Formal analysis: R.K.S.; Investigation: R.K.S.; Resources: O.J.T.; Data curation: R.K.S.; Writing - original draft: R.K.S.; Writing - review & editing: O.J.T.; Visualization: R.K.S.; Supervision: O.J.T.; Project administration: O.J.T.; Funding acquisition: O.J.T.

Funding
Research reported in this publication was supported by the National Institutes of Health: National Heart, Lung, and Blood Institute [R01HL142998 to O.J.T., T32HL027829 to R.K.S.] and the National Institute of Diabetes and Digestive and Kidney Diseases [K01DK103908 to O.J.T.]. It was also supported by an American Society of Hematology (ASH) Junior Faculty Scholar Award [O.J.T.]. Additional funding was provided by the University of Illinois at Chicago and the University of Wisconsin-Madison. Deposited in PMC for release after 12 months.

Data availability
Raw and processed scRNA-seq data have been deposited in the NCBI GEO database under accession number GSE186565.

References

Bahary, N., Goishi, K., Stuckenholz, C., Weber, G., Leblanc, J., Schafer, C. A., Berman, S. S., Klagsbrun, M. and Zon, L. I. (2007). Duplicate VegfA genes and orthologues of the KDR receptor tyrosine kinase family mediate vascular development in the zebrafish. *Blood* **110**, 3627-3636. doi:10.1182/blood-2006-04-016378

Batsivari, A., Rybtsov, S., Souilhol, C., Binagui-Casas, A., Hills, D., Zhao, S., Travers, P. and Medvinsky, A. (2017). Understanding hematopoietic stem cell development through functional correlation of their proliferative status with the intra-aortic cluster architecture. *Stem Cell Reports* **8**, 1549-1562. doi:10.1016/j.stemcr.2017.04.003

Bertrand, J. Y., Chi, N. C., Santoso, B., Teng, S., Stainier, D. Y. R. and Traver, D. (2010). Haematopoietic stem cells derive directly from aortic endothelium during development. *Nature* **464**, 108-111. doi:10.1038/nature08738

Boisset, J.-C., Van Cappellen, W., Andrieu-Soler, C., Galjart, N., Dzierzak, E. and Robin, C. (2010). In vivo imaging of haematopoietic cells emerging from the mouse aortic endothelium. *Nature* **464**, 116-120. doi:10.1038/nature08764

Bresciani, E., Broadbridge, E. and Liu, P. P. (2018). An efficient dissociation protocol for generation of single cell suspension from zebrafish embryos and larvae. *MethodsX* **5**, 1287-1290. doi:10.1016/j.mex.2018.10.009

Burger, A., Lindsay, H., Felker, A., Hess, C., Anders, C., Chiavacci, E., Zaugg, J., Weber, L. M., Catena, R., Jinek, M. et al. (2016). Maximizing mutagenesis with solubilized CRISPR-Cas9 ribonucleoprotein complexes. *Development* **143**, 2025-2037.

Chi, N. C., Shaw, R. M., De Val, S., Kang, G., Jan, L. Y., Black, B. L. and Stainier, D. Y. (2008). Foxn4 directly regulates tbx2b expression and atrioventricular canal formation. *Genes Dev* **22**, 734-739. doi:10.1101/gad.1629408

Ciau-Uitz, A., Monteiro, R., Kirmizitas, A. and Patient, R. (2014). Developmental hematopoiesis: Ontogeny, genetic programming and conservation. *Exp. Hematol.* **42**, 669-683. doi:10.1016/j.exphem.2014.06.001

Clement, K., Rees, H., Canver, M. C., Gehrke, J. M., Farouni, R., Hsu, J. Y., Cole, M. A., Liu, D. R., Joung, J. K., Bauer, D. E. et al. (2019). CRISPResso2 provides accurate and rapid genome editing sequence analysis. *Nat. Biotechnol.* **37**, 224-226. doi:10.1038/s41587-019-0032-3

Clements, W. K., Kim, A. D., Ong, K. G., Moore, J. C., Lawson, N. D. and Traver, D. (2011). A somitic Wnt16/Notch pathway specifies haematopoietic stem cells. *Nature* **474**, 220-224. doi:10.1038/nature10107

Covassin, L. D., Villefranc, J. A., Kacergis, M. C., Weinstein, B. M. and Lawson, N. D. (2006). Distinct genetic interactions between multiple Vegf receptors are required for development of different blood vessel types in zebrafish. *Proc. Natl. Acad. Sci. U S A* **103**, 6554-6559. doi:10.1073/pnas.0506886103

Ditadi, A., Sturgeon, C. M. and Keller, G. (2017). A view of human haematopoietic development from the Petri dish. *Nat. Rev. Mol. Cell Biol.* **18**, 56-67. doi:10.1038/nrm.2016.127

Duprey, S. P. and Boettiger, D. (1985). Developmental regulation of c-myb in normal myeloid progenitor cells. *Proc Natl Acad Sci U S A* **82**, 6937-6941. doi:10.1073/pnas.82.20.6937

Ellett, F., Pase, L., Hayman, J. W., Andrianopoulos, A. and Lieschke, G. J. (2011). mpeg1 promoter transgenes direct macrophage-lineage expression in zebrafish. *Blood* **117**, e49-e56. doi:10.1182/blood-2010-10-314120

Ellett, F., Elks, P. M., Robertson, A., Ogryzko, N. V. and Renshaw, S. (2015). Defining the phenotype of neutrophils following reverse migration in zebrafish. *J. Leukoc. Biol.* **98**, 975-981. doi:10.1189/jlb.3MA0315-105R

Ema, H. and Nakauchi, H. (2000). Expansion of hematopoietic stem cells in the developing liver of a mouse embryo. *Blood* **95**, 2284-2288. doi:10.1182/blood.V95.7.2284

Fang, S., Chen, S., Nurmi, H., Leppänen, V. M., Jeltsch, M., Scadden, D., Silberstein, L., Mikkola, H. and Alitalo, K. (2020). VEGF-C protects the integrity of the bone marrow perivascular niche in mice. *Blood* **136**, 1871-1883. doi:10.1182/blood.2020005699

Fang, S., Nurmi, H., Heinolainen, K., Chen, S., Salminen, E., Saharinen, P., Mikkola, H. K. A. and Alitalo, K. (2016). Critical requirement of VEGF-C in transition to fetal erythropoiesis. *Blood* **128**, 710-720. doi:10.1182/blood-2015-12-687970

Garcia-Porrero, J. A., Godin, I. E. and Dieterlen-Lièvre, F. (1995). Potential intraembryonic hemogenic sites at pre-liver stages in the mouse. *Anat. Embryol. (Berl)* **192**, 425-435.

Gazit, R., Garrison, B. S., Rao, T. N., Shay, T., Costello, J., Ericson, J., Kim, F., Collins, J. J., Regev, A., Wagers, A. J. et al. and **Immunological Genome Project Consortium** (2013). Transcriptome analysis identifies regulators of hematopoietic stem and progenitor cells. *Stem Cell Reports* **1**, 266-280. doi:10.1016/j.stemcr.2013.07.004

Gore, A. V., Swift, M. R., Cha, Y. R., Lo, B., Mckinney, M. C., Li, W., Castranova, D., Davis, A., Mukouyama, Y. S. and Weinstein, B. M. (2011). Rspo1/Wnt signaling promotes angiogenesis via Vegfc/Vegfr3. *Development* **138**, 4875-4886. doi:10.1242/dev.068460

Grimm, L., Nakajima, H., Chaudhury, S., Bower, N. I., Okuda, K. S., Cox, A. G., Harvey, N. L., Koltowska, K., Mochizuki, N. and Hogan, B. M. (2019). Yap1 promotes sprouting and proliferation of lymphatic progenitors downstream of Vegfc in the zebrafish trunk. *Elife* **8**, e42881. doi:10.7554/eLife.42881

Hall, C., Flores, M. V., Storm, T., Crosier, K. and Crosier, P. (2007). The zebrafish lysozyme C promoter drives myeloid-specific expression in transgenic fish. *BMC Dev. Biol.* **7**, 42. doi:10.1186/1471-213X-7-42

Hamada, K., Oike, Y., Takakura, N., Ito, Y., Jussila, L., Dumont, D. J., Alitalo, K. and Suda, T. (2000). VEGF-C signaling pathways through VEGFR-2 and VEGFR-3 in vasculoangiogenesis and hematopoiesis. *Blood* **96**, 3793-3800. doi:10.1182/blood.V96.12.3793

Hogan, B. M., Bos, F. L., Bussmann, J., Witte, M., Chi, N. C., Duckers, H. J. and Schulte-Merker, S. (2009). Ccbe1 is required for embryonic lymphangiogenesis and venous sprouting. *Nat. Genet.* **41**, 396-398. doi:10.1038/ng.321

Isles, H. M., Herman, K. D., Robertson, A. L., Loynes, C. A., Prince, L. R., Elks, P. M. and Renshaw, S. A. (2019). The CXCL12/CXCR4 signaling axis retains neutrophils at inflammatory sites in Zebrafish. *Front. Immunol.* **10**, 1784. doi:10.3389/fimmu.2019.01784

Jeltsch, M., Kaipainen, A., Joukov, V., Meng, X., Lakso, M., Rauvala, H., Swartz, M., Fukumura, D., Jain, R. K. and Alitalo, K. (1997). Hyperplasia of lymphatic vessels in VEGF-C transgenic mice. *Science* **276**, 1423-1425. doi:10.1126/science.276.5317.1423

Jin, H., Xu, J. and Wen, Z. (2007). Migratory path of definitive hematopoietic stem/progenitor cells during zebrafish development. *Blood* **109**, 5208-5214. doi:10.1182/blood-2007-01-069005

Jin, H., Sood, R., Xu, J., Zhen, F., English, M. A., Liu, P. P. and Wen, Z. (2009). Definitive hematopoietic stem/progenitor cells manifest distinct differentiation output in the zebrafish VDA and PBI. *Development* **136**, 647-654. doi:10.1242/dev.029637

Joukov, V., Pajusola, K., Kaipainen, A., Chilov, D., Lahtinen, I., Kukk, E., Saksela, O., Kalkkinen, N. and Alitalo, K. (1996). A novel vascular endothelial growth factor, VEGF-C, is a ligand for the Flt4 (VEGFR-3) and KDR (VEGFR-2) receptor tyrosine kinases. *EMBO J.* **15**, 1751. doi:10.1002/j.1460-2075.1996.tb00521.x

Joukov, V., Sorsa, T., Kumar, V., Jeltsch, M., Claesson-Welsh, L., Cao, Y., Saksela, O., Kalkkinen, N. and Alitalo, K. (1997). Proteolytic processing regulates receptor specificity and activity of VEGF-C. *EMBO J.* **16**, 3898-3911. doi:10.1093/emboj/16.13.3898

Kang, H., Mesquitta, W. T., Jung, H. S., Moskvin, O. V., Thomson, J. A. and Slukvin, I. I. (2018). GATA2 is dispensable for specification of hemogenic endothelium but promotes endothelial-to-hematopoietic transition. *Stem Cell Reports* **11**, 197-211. doi:10.1016/j.stemcr.2018.05.002

Karkkainen, M. J., Haiko, P., Sainio, K., Partanen, J., Taipale, J., Petrova, T. V., Jeltsch, M., Jackson, D. G., Talikka, M., Rauvala, H. et al. (2004). Vascular endothelial growth factor C is required for sprouting of the first lymphatic vessels from embryonic veins. *Nat. Immunol.* **5**, 74-80. doi:10.1038/ni1013

Kissa, K. and Herbomel, P. (2010). Blood stem cells emerge from aortic endothelium by a novel type of cell transition. *Nature* **464**, 112-115. doi:10.1038/nature08761

Kissa, K., Murayama, E., Zapata, A., Cortés, A., Perret, E., Machu, C. and Herbomel, P. (2008). Live imaging of emerging hematopoietic stem cells and early thymus colonization. *Blood* **111**, 1147-1156. doi:10.1182/blood-2007-07-099499

Kobayashi, I., Kobayashi-Sun, J., Kim, A. D., Pouget, C., Fujita, N., Suda, T. and Traver, D. (2014). Jam1a-Jam2a interactions regulate haematopoietic stem cell fate through Notch signalling. *Nature* **512**, 319-323. doi:10.1038/nature13623

Kobayashi, I., Kondo, M., Yamamori, S., Kobayashi-Sun, J., Taniguchi, M., Kanemaru, K., Katakura, F. and Traver, D. (2019). Enrichment of hematopoietic stem/progenitor cells in the zebrafish kidney. *Sci Rep* **9**, 14205. doi:10.1038/s41598-019-50672-5

Kobayashi-Osaki, M., Ohneda, O., Suzuki, N., Minegishi, N., Yokomizo, T., Takahashi, S., Lim, K. C., Engel, J. D. and Yamamoto, M. (2005). GATA motifs regulate early hematopoietic lineage-specific expression of the Gata2 gene. *Mol. Cell Biol.* **25**, 7005-7020. doi:10.1128/MCB.25.16.7005-7020.2005

Küchler, A. M., Gjini, E., Peterson-Maduro, J., Cancilla, B., Wolburg, H. and Schulte-Merker, S. (2006). Development of the zebrafish lymphatic system requires VEGFC signaling. *Curr. Biol.* **16**, 1244-1248. doi:10.1016/j.cub.2006.05.026

Kwon, H.-B., Fukuhara, S., Asakawa, K., Ando, K., Kashiwada, T., Kawakami, K., Hibi, M., Kwon, Y.-G., Kim, K.-W., Alitalo, K. et al. (2013). The parallel growth of motoneuron axons with the dorsal aorta depends on Vegfc/Vegfr3 signaling in zebrafish. *Development* **140**, 4081-4090. doi:10.1242/dev.091702

Lancino, M., Majello, S., Herbert, S., De Chaumont, F., Tinevez, J.-Y., Olivo-Marin, J.-C., Herbomel, P. and Schmidt, A. (2018). Anisotropic organization of circumferential actomyosin characterizes hematopoietic stem cells emergence in the zebrafish. *eLife* **7**, 1131. doi:10.7554/eLife.37355

Le Guen, L., Karpanen, T., Schulte, D., Harris, N. C., Koltowska, K., Roukens, G., Bower, N. I., Van Impel, A., Stacker, S. A., Achen, M. G. et al. (2014). Ccbe1 regulates Vegfc-mediated induction of Vegfr3 signaling during embryonic lymphangiogenesis. *Development* **141**, 1239-1249. doi:10.1242/dev.100495

Li, L., Yan, B., Shi, Y.-Q., Zhang, W.-Q. and Wen, Z.-L. (2012). Live imaging reveals differing roles of macrophages and neutrophils during zebrafish tail fin regeneration. *J. Biol. Chem.* **287**, 25353-25360. doi:10.1074/jbc.M112.349126

Liao, E. C., Paw, B. H., Oates, A. C., Pratt, S. J., Postlethwait, J. H. and Zon, L. I. (1998). SCL/Tal-1 transcription factor acts downstream of cloche to specify hematopoietic and vascular progenitors in zebrafish. *Genes Dev.* **12**, 621-626. doi:10.1101/gad.12.5.621

Lieschke, G. J., Oates, A. C., Crowhurst, M. O., Ward, A. C. and Layton, J. E. (2001). Morphologic and functional characterization of granulocytes and macrophages in embryonic and adult zebrafish. *Blood* **98**, 3087-3096. doi:10.1182/blood.V98.10.3087

Lin, H.-F., Traver, D., Zhu, H., Dooley, K., Paw, B. H., Zon, L. I. and Handin, R. I. (2005). Analysis of thrombocyte development in CD41-GFP transgenic zebrafish. *Blood* **106**, 3803-3810. doi:10.1182/blood-2005-01-0179

Mathias, J. R., Perrin, B. J., Liu, T.-X., Kanki, J., Look, A. T. and Huttenlocher, A. (2006). Resolution of inflammation by retrograde chemotaxis of neutrophils in transgenic zebrafish. *J. Leukoc. Biol.* **80**, 1281-1288. doi:10.1189/jlb.0506346

Miskolci, V., Squirrell, J., Rindy, J., Vincent, W., Sauer, J. D., Gibson, A., Eliceiri, K. W. and Huttenlocher, A. (2019). Distinct inflammatory and wound healing responses to complex caudal fin injuries of larval zebrafish. *eLife* **8**, e45976. doi:10.7554/eLife.45976

Müller, A. M., Medvinsky, A., Strouboulis, J., Grosveld, F. and Dzierzak, E. (1994). Development of hematopoietic stem cell activity in the mouse embryo. *Immunity* **1**, 291-301. doi:10.1016/1074-7613(94)90081-7

Murayama, E., Kissa, K., Zapata, A., Mordelet, E., Briolat, V., Lin, H.-F., Handin, R. I. and Herbomel, P. (2006). Tracing hematopoietic precursor migration to successive hematopoietic organs during Zebrafish development. *Immunity* **25**, 963-975. doi:10.1016/j.immuni.2006.10.015

Ninov, N., Borius, M. and Stainier, D. Y. (2012). Different levels of Notch signaling regulate quiescence, renewal and differentiation in pancreatic endocrine progenitors. *Development* **139**, 1557-1567. doi:10.1242/dev.076000

North, T., Gu, T. L., Stacy, T., Wang, Q., Howard, L., Binder, M., Marín-Padilla, M. and Speck, N. A. (1999). Cbfa2 is required for the formation of intra-aortic hematopoietic clusters. *Development* **126**, 2563-2575. doi:10.1242/dev.126.11.2563

North, T. E., Goessling, W., Walkley, C. R., Lengerke, C., Kopani, K. R., Lord, A. M., Weber, G. J., Bowman, T. V., Jang, I.-H., Grosser, T. et al. (2007). Prostaglandin E2 regulates vertebrate haematopoietic stem cell homeostasis. *Nature* **447**, 1007-1011. doi:10.1038/nature05883

Ober, E. A., Olofsson, B., Mäkinen, T., Jin, S.-W., Shoji, W., Koh, G. Y., Alitalo, K. and Stainier, D. Y. R. (2004). Vegfc is required for vascular development and endoderm morphogenesis in zebrafish. *EMBO Rep.* **5**, 78-84. doi:10.1038/sj.embor.7400047

Pardanaud, L. and Dieterlen-Lièvre, F. (1999). Manipulation of the angiopoietic/hemangiopoietic commitment in the avian embryo. *Development* **126**, 617-627. doi:10.1242/dev.126.4.617

Peeters, M., Ottersbach, K., Bollerot, K., Orelio, C., De Bruijn, M., Wijgerde, M. and Dzierzak, E. (2009). Ventral embryonic tissues and Hedgehog proteins induce early AGM hematopoietic stem cell development. *Development* **136**, 2613-2621. doi:10.1242/dev.034728

Rosowski, E. E., Raffa, N., Knox, B. P., Golenberg, N., Keller, N. P. and Huttenlocher, A. (2018). Macrophages inhibit Aspergillus fumigatus germination and neutrophil-mediated fungal killing. *PLOS Pathogens* **14**, e1007229. doi:10.1371/journal.ppat.1007229

Seita, J., Sahoo, D., Rossi, D. J., Bhattacharya, D., Serwold, T., Inlay, M. A., Ehrlich, L. I., Fathman, J. W., Dill, D. L. and Weissman, I. L. (2012). Gene expression commons: an open platform for absolute gene expression profiling. *PLoS ONE* **7**, e40321. doi:10.1371/journal.pone.0040321

Serbedzija, G. N., Flynn, E. and Willett, C. E. (1999). Zebrafish angiogenesis: a new model for drug screening. *Angiogenesis* **3**, 353-359. doi:10.1023/A:1026598300052

Sheehan, H. L. and Storey, G. W. (1947). An improved method of staining leucocyte granules with Sudan black B. *J Pathol Bacteriol.* **59**, 336. doi:10.1002/path.1700590142

Shin, M., Beane, T. J., Quillien, A., Male, I., Zhu, L. J. and Lawson, N. D. (2016). Vegfa signals through ERK to promote angiogenesis, but not artery differentiation. *Development* **143**, 3796-3805.

Slukvin, I. I. (2013). Hematopoietic specification from human pluripotent stem cells: current advances and challenges toward de novo generation of hematopoietic stem cells. *Blood* **122**, 4035-4046. doi:10.1182/blood-2013-07-474825

Stacker, S. A., Williams, S. P., Karnezis, T., Shayan, R., Fox, S. B. and Achen, M. G. (2014). Lymphangiogenesis and lymphatic vessel remodelling in cancer. *Nat. Rev. Cancer* **14**, 159-172. doi:10.1038/nrc3677

Stuart, T., Butler, A., Hoffman, P., Hafemeister, C., Papalexi, E., Mauck, W. M., III, Hao, Y., Stoeckius, M., Smibert, P. and Satija, R. (2019). Comprehensive integration of single-cell data. *Cell* **177**, 1888-1902.e21. doi:10.1016/j.cell.2019.05.031

Sukbuntherng, J., Cropp, G., Hannah, A., Wagner, G. S., Shawver, L. K. and Antonian, L. (2001). Pharmacokinetics and interspecies scaling of a novel VEGF receptor inhibitor, SU5416. *J. Pharm. Pharmacol.* **53**, 1629-1636. doi:10.1211/0022357011778232

Tamplin, O. J., Durand, E. M., Carr, L. A., Childs, S. J., Hagedorn, E. J., Li, P., Yzaguirre, A. D., Speck, N. A. and Zon, L. I. (2015). Hematopoietic stem cell arrival triggers dynamic remodeling of the perivascular niche. *Cell* **160**, 241-252. doi:10.1016/j.cell.2014.12.032

Thisse, C. and Thisse, B. (2008). High-resolution in situ hybridization to whole-mount zebrafish embryos. *Nat. Protocols* **3**, 59-69. doi:10.1038/nprot.2007.514

Villefranc, J. A., Nicoli, S., Bentley, K., Jeltsch, M., Zarkada, G., Moore, J. C., Gerhardt, H., Alitalo, K. and Lawson, N. D. (2013). A truncation allele in vascular endothelial growth factor c reveals distinct modes of signaling during lymphatic and vascular development. *Development* **140**, 1497-1506. doi:10.1242/dev.084152

Vogrin, A. J., Bower, N. I., Gunzburg, M. J., Roufail, S., Okuda, K. S., Paterson, S., Headey, S. J., Stacker, S. A., Hogan, B. M. and Achen, M. G. (2019). Evolutionary differences in the Vegf/Vegfr code reveal organotypic roles for the endothelial cell receptor Kdr in developmental lymphangiogenesis. *Cell Rep* **28**, 2023-2036.e4. doi:10.1016/j.celrep.2019.07.055

Wang, G., Muhl, L., Padberg, Y., Dupont, L., Peterson-Maduro, J., Stehling, M., Le Noble, F., Colige, A., Betsholtz, C., Schulte-Merker, S. et al. (2020). Specific fibroblast subpopulations and neuronal structures provide local sources of Vegfc-processing components during zebrafish lymphangiogenesis. *Nat. Commun.* **11**, 2724. doi:10.1038/s41467-020-16552-7

Westerfield, M. (2000). *The Zebrafish Book. A Guide for the Laboratory Use of Zebrafish (Danio rerio)*. Eugene, OR: University of Oregon Press.

Willett, C. E., Zapata, A. G., Hopkins, N. and Steiner, L. A. (1997). Expression of ZebrafishragGenes during early development identifies the thymus. *Dev. Biol.* **182**, 331-341. doi:10.1006/dbio.1996.8446

Yokomizo, T. and Dzierzak, E. (2010). Three-dimensional cartography of hematopoietic clusters in the vasculature of whole mouse embryos. *Development* **137**, 3651-3661. doi:10.1242/dev.051094

Zhu, Q., Gao, P., Tober, J., Bennett, L., Chen, C., Uzun, Y., Li, Y., Howell, E. D., Mumau, M., Yu, W. et al. (2020). Developmental trajectory of prehematopoietic stem cell formation from endothelium. *Blood* **136**, 845-856. doi:10.1182/blood.2020004801

Zou, Z., Enis, D. R., Bui, H., Khandros, E., Kumar, V., Jakus, Z., Thom, C., Yang, Y., Dhillon, V., Chen, M. et al. (2013). The secreted lymphangiogenic factor CCBE1 is essential for fetal liver erythropoiesis. *Blood* **121**, 3228-3236. doi:10.1182/blood-2012-10-462689